Search for gauge-mediated supersymmetry in events with photons and a Z boson decaying to charged leptons at CMS

von
Sebastian Wuchterl

Masterarbeit in Physik

vorgelegt der
Fakultät für Mathematik, Informatik und Naturwissenschaften der
RWTH Aachen

im
xx 2018

angefertigt im
I. Physikalischem Institut B

bei
Prof. Dr. Lutz Feld

Contents

1 Introduction **5**
1.1 System of units . . . 5
1.2 The standard model of particle physics . . . 5
1.2.1 Indications for physics beyond the standard model . . . 7
1.3 Supersymmetry . . . 8
1.3.1 General gauge mediation . . . 11
1.3.2 Signal scenarios . . . 11
1.3.3 Status of SUSY searches at the Large Hadron Collider . . . 13

2 The Experiment **17**
2.1 The large hadron collider . . . 17
2.2 The compact muon solenoid detector . . . 19
2.2.1 Tracker system . . . 19
2.2.2 Electromagnetic calorimeter . . . 21
2.2.3 Hadronic calorimeter . . . 22
2.2.4 The solenoid . . . 23
2.2.5 Muon system . . . 23
2.2.6 Trigger system . . . 24

Bibliography **25**

Chapter 1

Introduction

TODO September 26, 2018: EinleitungssÃtze for jedem Chapter

1.1 System of units

For simplicity, the unit system commonly used in particle physics is the natural unit system [1]. In natural units, the reduced Planck constant $\hbar$ and the speed of light c are set to unity:

$$\hbar = c = 1 \tag{1.1}$$

The observables used most frequently in particle physics are the energy, momentum, and mass. They are given in GeV in the natural unit system. For other variables, such as length and time, the metric unit system is used. Cross sections are given in barn ($1\,\mathrm{b} = 10^{-28}\,\mathrm{m}^2$). Integrated luminosities are therefore given in b^{-1}.

1.2 The standard model of particle physics

The standard model of particle physics (SM) is a gauge theory describing three of the four fundamental forces, namely the electromagnetic, weak, and strong interaction [2]. The gravitational force is described by general relativity [3].
All fundamental particles can be divided into two sub classes: Particles of integer spin, called bosons, and particles of half-integer spin, called fermions.

The SM is based on the symmetry group $SU(3) \otimes SU(2) \otimes U(1)$. The interactions are described via the exchange of spin-1 gauge fields, namely being the bosons. In the case of the strong force these are 8 massless gluons, which couple to the color charge. The mediator of the electromagnetic interaction is the massless photon, coupling to the electric charge of particles. And for the weak interaction, these are the three massive bosons $W^{\pm}$ and Z, which couple to weak charge.

While the bosons describe the mediation of the fundamental forces, the matter content is given by the fermions. Fermions are divided into two subgroups, called quarks and leptons. Leptons take part only in the electroweak interaction, while quarks carry also

a color charge and therefore interact via the strong force. There are three generations of fermions, which include each two lepton and two quark flavors. The quark flavors are namely the down, up, strange, charm, bottom, and top quarks, while the lepton flavors are made up of three electrically charged particles, the electron (e), the muon (μ), and the tau lepton (τ), and three electric neutral leptons, called neutrinos (ν_e, ν_μ, ν_τ). The latter are assigned the names of the charged leptons of the same generation. Of the quarks, there are up-type quarks carrying an electric charge of $+\frac{2}{3}e$, and down-type quarks carrying an electric charge of $-\frac{1}{3}e$.
An illustration of the total SM particle content with its properties is shown in Figure 1.1. For each particle, a corresponding anti-particle exists with same mass and inversed quantum numbers. Throughout this thesis particles and antiparticles will be treated the same way, and will be labeled with the name of the particle.

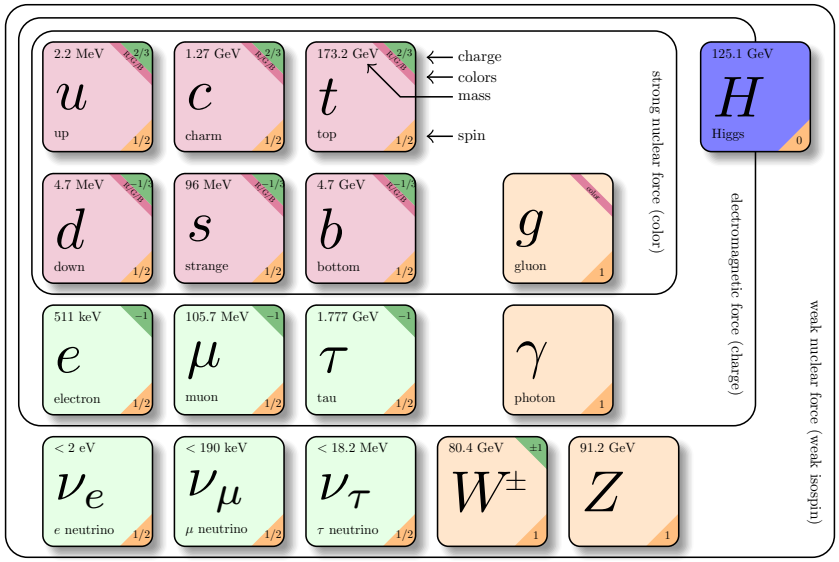

Figure 1.1: Total particle content of the standard model. For each particle important properties such as mass, spin, and charges are given. The values are taken from [4].

The strong interaction between quarks and gluons is described by the quantum field theory of quantum chromodynamics (QCD). The corresponding mediators of the non-abelian gauge group $SU(2)_C$ are the eight gluons, which carry each the color-charge C of an anti-color and color, giving rise to the self coupling of gluons. Due to the confinement of quarks [5], quark-antiquark pairs will be produced out of the vacuum, if particles with color charge are being separated, since the potential energy density of the strong force includes constant terms, and the potential energy rises with increasing distance. The same principle leads to the existence of only color-neutral bound states of two (mesons), or three (baryons) quarks, called hadrons.

The electromagnetic and weak force can be unified in the electroweak theory to obtain the electroweak interaction [6–9], represented by the gauge group $SU(2)_L \otimes U(1)_Y$. The indices L and Y indicate, that the weak isospin T couples only to lefthanded $SU(2)_L$ doublets of fermions, while the righthanded $SU(2)_L$ singlets carry no isospin, and Y is the hypercharge. The three mediators of the $SU(2)_L$ group are the W^1, W^2, and W^3 bosons, and the gauge boson of the $U(1)_Y$ group is the B^0 boson. Due to the spontaneous symmetry breaking in the electroweak unification, these four bosons mix to the observed $W^\pm$ and Z boson, and the photon γ:

$$\begin{pmatrix} \gamma \\ Z \end{pmatrix} = \begin{pmatrix} \cos(\theta_W) & \sin(\theta_W) \\ -\sin(\theta_W) & \cos(\theta_W) \end{pmatrix} \cdot \begin{pmatrix} B \\ W^3 \end{pmatrix} \tag{1.2}$$

$$W^\pm = \frac{1}{\sqrt{2}} \left(W^1 \mp i W^2 \right) \tag{1.3}$$

The resulting weak interaction is parity violating. The $W^\pm$ bosons only couple to lefthanded fermions, while the neutral Z boson couples to both lefthanded and righthanded particles, but with different strength.

Because in this theory the gauge bosons are not allowed to have masses, the Higgs mechanism is introduced [10–12]. It predicts a complex scalar doublet Higgs field, which is symmetric, but has a non zero vacuum expectation value and is therefore responsible for the spontaneous symmetry breaking of the $SU(2)_L \otimes U(1)_Y$ gauge group. Since it has four degrees of freedom, but only three are used to give masses to the $W^\pm$ and the Z bosons, a fourth spin-0 boson is postulated, namely the Higgs boson. Leptons acquire also masses in the SM via Yukawa couplings with the Higgs field. Such a spin-0 neutral boson has been observed in proton-proton collisions at the LHC in 2012 [13, 14], and its mass has been determined to be $125.09 \pm 0.24\,\text{GeV}$. This theory earned validation in good agreement with SM predictions [15], and recently also couplings to the top quark [16], and decays to bottom quarks and tau leptons have been observed [17, 18], strengthening the presumption, that the found boson is the postulated Higgs boson.

1.2.1 Indications for physics beyond the standard model

Although the SM describes all phenomena observed at high energy particle colliders successfully, different observations indicate that there must exist physics beyond the standard model (BSM).
Precise measurements of the cosmic microwave background and theoretical interpretations suggest, that only 4.9% of the universe consist of ordinary matter, while the remainder is composited of dark energy and dark matter [19]. The existence of dark matter is also observed in gravitational lensing effects [20], and in rotation curves of spiral galaxies [21]. But inside the SM, there exists no particle, that could explain the total amount of dark matter in the universe.
It is assumed, that in the early age of the universe there was the same amount of matter

and antimatter. But, today we observe the existence of much more matter than antimatter [22, 23]. In order do explain this discrepancy, different conditions, such as $\mathcal{CP}$-violation and baryon number violation, should be fulfilled [24]. However, there are no known sources of violation effects large enough to give rise to such big differences.
In the SM, neutrinos are assumed to be massless particles. But, the observation of neutrino oscillations are only explicable if neutrinos are massive particles [4, 25].
The observation of the Higgs boson in 2012 on the one hand marks the great success of the SM, but on the other hand directly leads to a big problem concerning the Higgs mass, what is known as the "Hierarchy Problem". The Higgs boson couples to all massive particles, and the coupling strength is proportional to their masses. But unlike for all other particles, the mass term for the Higgs boson is quadratically divergent, caused by virtual loop corrections from the fermion couplings. The cut-off scale for these corrections can be as large as the validity of the SM. Thus, the Higgs boson mass can be pushed to the order of the Planck scale (10^{19} GeV). Since its mass was measured at the LHC to be ≈ 125 GeV, and the difference between the electroweak scale (10^2 GeV) and the Planck scale is that huge, these corrections terms need to cancel per coincidence. This is considered as "unnatural", leading to the expectation that new physics is hiding in the energy ranges up to the Planck scale.
Also, driven by the electroweak unification, the unification of all forces in a grand unified theory (GUT) is well motivated. Because the couplings of the forces in the SM do not lead to a unification at very high energies [4], a possible extension of the SM with additional new particles could explain such a unification of the electroweak and strong interaction. One of those theories is supersymmetry [26].

1.3 Supersymmetry

Supersymmetry (SSM) [26, 27] is one of the most popular BSM models and was developed already in the 1970s. It is well motivated within theory, because it is the only possible extension of space time symmetry. Since then, many different SUSY models have been established, all based on the same principle: SUSY connects fermions with bosons and the other way around by introducing supersymmetric partners for each SM particle. These superpartners differ only in spin by $\pm 1/2$, all other quantum numbers are kept equal. With the help of generators Q_i, bosonic and fermionic states can be switched:

$$Q|fermion\rangle = |boson\rangle, \qquad +Q|boson\rangle = |fermion\rangle \tag{1.4}$$

Some of the many advantages of SUSY are, that multiple models directly provide candidates for dark matter particles, solve the unification of forces and the Hierarchy Problem without any "fine tuning".
The simplest form of SUSY is the minimal supersymmetric standard model (MSSM), where only exactly one pair of $Q, \dagger Q$ exists. So within the MSSM, for each fermion in the SM a supersymmetric scalar boson is introduced. To differentiate between these two, the names of supersymmetric partners are those of the SM particles prepended with an "s-" (standing for scalar). The partners of fermions are called sfermions, and e.g. the partner

of the electron is the selectron. The names of superpartners of the bosons are created by appending the SM with an "-ino", making them bosinos, and the partner of the gluon for example is called gluino. In general, the superpartners are called sparticles, and are labeled the same as their SM counterparts, but with a tilde ($\mu \to \widetilde{\mu}$).
To give masses in the spontaneous symmetry breaking to all particles and sparticles, the SM higgs sector needs to be extended to two complex scalar doublets:

$$H_u = \begin{bmatrix} H_u^+ \\ H_u^0 \end{bmatrix}, \qquad H_d = \begin{bmatrix} H_d^0 \\ H_d^- \end{bmatrix} \tag{1.5}$$

The H_d gives masses to the down-type quarks and charged leptons, while the H_u is responsible for the masses of up-type quarks. Consistently four higgsinos as superpartners are introduced in the MSSM. In the spontaneous symmetry breaking there are eight degrees of freedom instead of four, coming from the two Doublets, and giving rise to an expanded Higgs sector consisting of five particles: the two neutral scalars h^0 and H^0, the two charged scalars $H^\pm$, and the neutral pseudoscalar A^0. The observed Higgs boson at the LHC can be identified as one of the two neutral scalars, where the lighter h^0 is chosen by convention.
The gauginos and higgsinos mix, similar to the mixing in the electroweak sector, to six mass eigenstates, which are the four neutral neutralinos $\widetilde{\chi}_1^0$, $\widetilde{\chi}_2^0$, $\widetilde{\chi}_3^0$, and $\widetilde{\chi}_4^0$, and the two charged charginos $\widetilde{\chi}_1^\pm$ and $\widetilde{\chi}_2^+$.
The total particle content of the MSSM is shown in Figure 1.2. As an extension and to include gravity, the SM is extended by the graviton G, and the SUSY sector by its superpartner, the gravitino $\widetilde{G}$.

Because in an unbroken symmetry the particles and their corresponding sparticles should posses the same masses, and those SUSY particles should have been found easily in the past (considering e.g. an electron/selectron mass of $\approx 511\,\mathrm{keV}$), SUSY must be a broken symmetry. There have been many different theories developed over time to explain different breaking scenarios.
SUSY can provide Dark Matter candidates, if the lightest supersymmetric particle (LSP), is stable, electrically neutral, and uncolored. But, it is not fundamentally necessary, that the LSP is stable. In so-called R-Parity violating scenarios, decays of all SUSY particles into SM particles are allowed. Hence, the conservation of the Baryon number B, and the lepton number L is violated. The R-parity

$$R = (-1)^{3B+L+S} \tag{1.6}$$

is therefore introduced as a new quantum number, where S is the spin. The R-parity is -1 for sparticles, and $+1$ for particles respectively. R-parity conserving scenarios are motivated by many precision measurements, such as the life time measurement of the proton [28]. In this thesis, only R-parity conserving scenarios are considered.

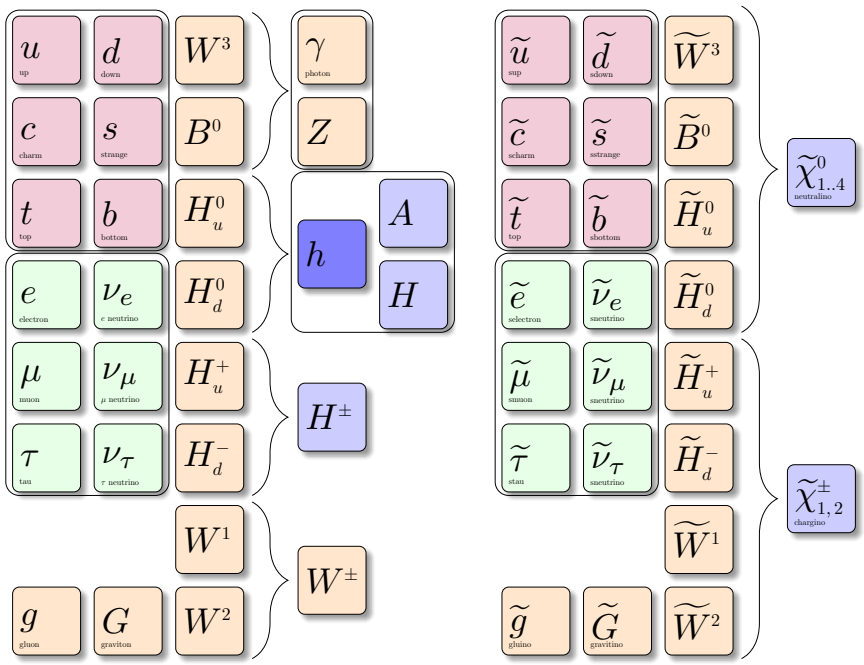

Figure 1.2: The particle content of the MSSM extended with the graviton and gravitino. Mixings to mass eigenstates are indicates with the brackets.

1.3.1 General gauge mediation

The phenomenology of SUSY is very rich. While most of the popular models gravity is responsible for the SUSY breaking, a different approach, also motivating this search, is general gauge mediation (GGM) [29]. In these gauge mediated supersymmetry breaking (GMSB) models, an additional "hidden sector" is introduced, which is responsible for the breaking. This sector is mainly decoupled, and the possible interactions between the visible and the hidden sector are only achieved by messenger fields mediated by gauge interactions. In GMSB, the LSP is typically the gravitino $\widetilde{G}$, and this particle is assumed to be very light ($\ll 1\,\text{GeV}$). Therefore, the next-to-lightest supersymmetric particle (NLSP), which can be basically any sparticle, decays promptly. Since the gravitino is stable because of R-parity conservation, electrically and color neutral, it will leave any detector undetected, causing an imbalance in the measured total transverse momentum in proton-proton collisions of the LHC.
In all models considered throughout this thesis, the NLSP is assumed to be the lightest neutralino ($\widetilde{\chi}_1^0$). The mixing of the NLSP can include bino, wino, and higgsino components, each enabling different decay channels.

1.3.2 Signal scenarios

Given the theoretical background, the signal scenarios considered in this thesis are discussed in the following. All couplings of the SUSY particles are the same as of their SM partners. Hence, very different production channels, such as electroweak and strong production, are possible. In case of the LHC proton-proton collisions, SUSY particles are typically produced directly in the hard process, leading to cascade like decay structures down to the decays of the NLSP to the gravitino and a SM boson. The branching fractions of the lightest neutralino to different SM bosons depends on its mixing

$$\widetilde{\chi}_1^0 = \sum_{i=1}^{N} N_1 \widetilde{\psi}_i^0, \tag{1.7}$$

where $\widetilde{\psi}_i^0 = (\widetilde{B}, \widetilde{W}, \widetilde{H}_d^0, \widetilde{H}_u^0)$ [30]. The mass eigenstate vectors N_i are defined through four parameters, the bino mass M_1 and wino mass M_2 at the messenger scale, the supersymmetric mass term for Higgs μ, and $\tan\beta$, the ratio between the two vacuum expectation values of the up- and down type Higgs. In general a neutralino NLSP has three possible decays, all involving the $\widetilde{G}$:

$$\Gamma\left(\widetilde{\chi}_1^0 \to \widetilde{G} + \gamma\right) = |N_{11}c_W + N_{12}s_W|^2 \mathcal{A} \tag{1.8}$$

$$\Gamma\left(\widetilde{\chi}_1^0 \to \widetilde{G} + Z\right) = \left(|N_{12}c_W - N_{11}s_W|^2 + \frac{1}{2}|N_{13}c_\beta - N_{14}s_\beta|^2\right)\left(1 - \frac{m_Z^2}{m_{\widetilde{\chi}_1^0}^2}\right)^4 \mathcal{A} \tag{1.9}$$

$$\Gamma\left(\widetilde{\chi}_1^0 \to \widetilde{G} + h\right) = \frac{1}{2}|N_{13}c_\beta + N_{14}s_\beta|^2 \left(1 - \frac{m_h^2}{m^2}\right)^4 \mathcal{A} \tag{1.10}$$

Here, c_W, s_W, c_β, and s_β are abbreviations for $\cos(\theta_{Weinberg})$, $\sin(\theta_{Weinberg})$, $\cos(\beta)$, and $\sin(\beta)$. The formulae hold in cases of onshell Z and h production. $\mathcal{A}$ is a parameter responsible for the NLSP lifetime [31, 32]

$$\mathcal{A} = \frac{m^5_{\widetilde{\chi}^0_1}}{16\pi F_0^2} \approx \left(\frac{m_{\widetilde{\chi}^0_1}}{100\,\text{GeV}}\right)^5 \left(\frac{100\,\text{TeV}}{\sqrt{F_0}}\right)^4 \frac{1}{0.1\,\text{mm}}, \tag{1.11}$$

where F_0 is the scale of SUSY breaking, its range is given by $10\,\text{TeV} \lesssim \sqrt{F_0} \lesssim 10^6\,\text{TeV}$, and it is related to the gravitino mass via $m_{\widetilde{G}} = \frac{F_0}{\sqrt{3}M_{Planck}}$.
Branching fractions for pure bino, wino and higgsino like NLSPs are shown in Figure 1.3. Since the final state investigated in this analysis consists of a Z boson and a photon, the search is sensitive in particular to bino and wino like NLSP scenarios.
One scenario used in the development of this search, is a full GGM model, where the NLSP is the $\widetilde{\chi}^0_1$, and it is assumed to be 100% bino like. The heavier neutralino $\widetilde{\chi}^0_2$, and the lightest chargino $\widetilde{\chi}^\pm_1$, are assumed to be 100% wino like. Therefore, the bino mass equals the mass of the lightest neutralino mass, while the $\widetilde{\chi}^+_1$ and the $\widetilde{\chi}^0_2$ are mass degenerate and their mass equals the wino mass. For simplification reasons higgsinos are decoupled, i.e. set to very high masses. Squarks and gluinos are also decoupled in this scenario, allowing only electroweak production modes. For the most dominant process a diagram is shown in Fig. Figure 1.4. The signal cross section depends only on the wino mass, since $\widetilde{\chi}^0_1\widetilde{\chi}^+_1$ and $\widetilde{\chi}^+_1\widetilde{\chi}^+_1$ are by far the most dominant production scenarios. The branching fractions of the gauginos are given by the gaugino masses and their gauge eigenstates, and behave exactly like shown in Figure 1.3. The mass of the neutralinos and the lightest chargino directly influence the transverse momenta in the final state. As can be seen in Figure 1.4, larger mass differences between the NLSP mass and the wino mass lead to higher momenta of the produced bosons in the cascades. The mass of the NLSP directly is responsible for the momenta of the final SM bosons and the gravitino, and therefore directly the missing transverse momentum in an event.

A very different approach besides analyzing full theoretical models, are simplified models (SMS)[33]. Here, only a limited particle content is assumed with simplified assumptions on the mixings and decay channels, providing a more model independent result via probing specifically distinct final states. These results can therefore be reinterpreted in various different general models, because fixed production channels and fixed branching fractions are used [34]. In this thesis, two simplified models are considered, one with electroweak production, and the other one with a strong production channel.
The electroweak model is the TChiZG SMS, in which only neutralino-chargino and chargino-chargino production is assumed. The lightest chargino and lightest neutralino are set to have nearly the same mass, leading to soft emissions of offshell W bosons in the decays of the charginos to the NLSP. The branching fractions of the lightest neutralino to a gravitino and a photon or a Z boson are fixed to 50% each ($\mathcal{BR}(\widetilde{\chi}^0_1 \to \gamma) = \mathcal{BR}(\widetilde{\chi}^0_1 \to Z) = 0.5$). A diagram for the process can be found in Figure 1.4. The squarks and gluinos are decoupled.
The strong model considered here is the T5bbbbZG SMS. A diagram can be found in

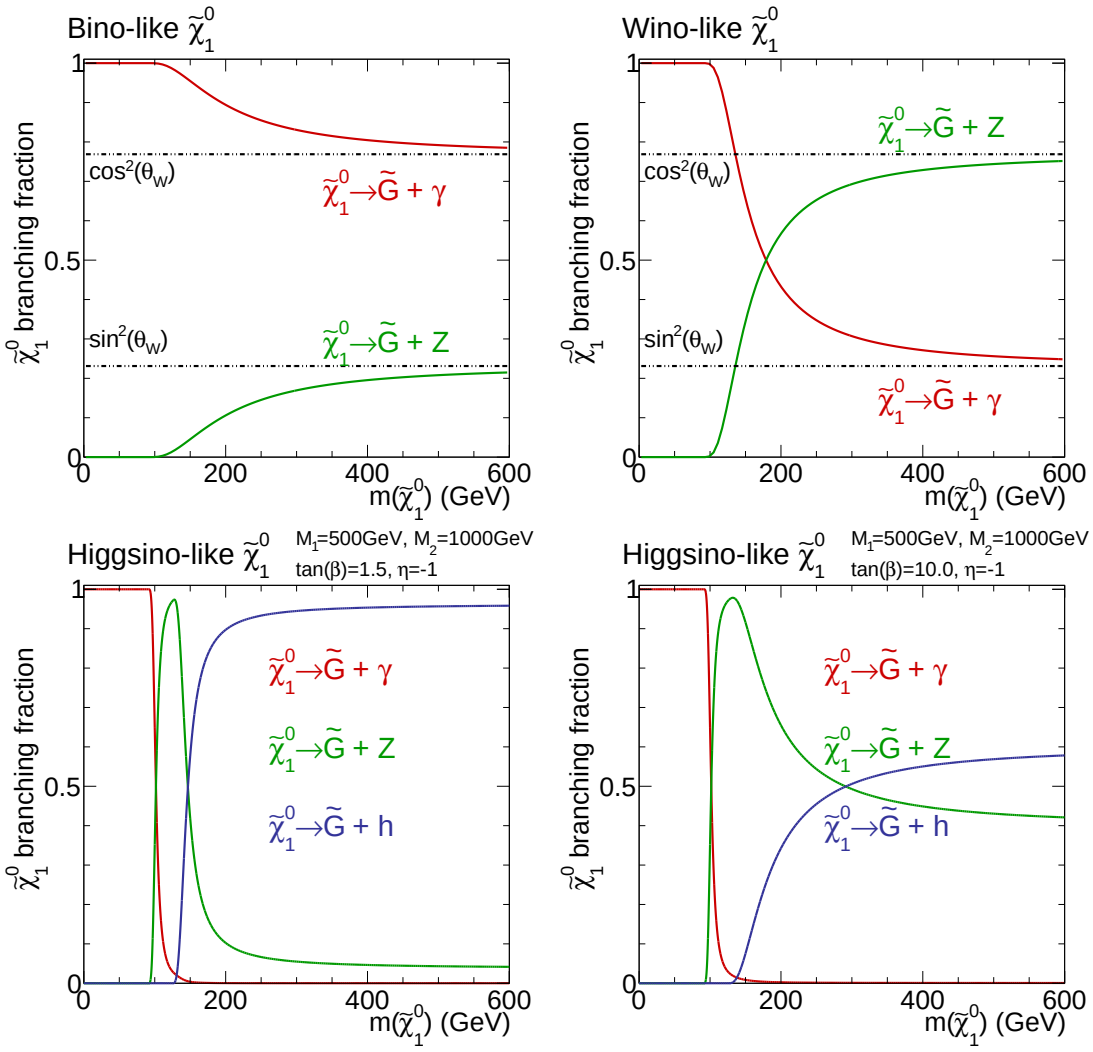

Figure 1.3: Branching fractions for pure bino (top left), wino (top right), and two higgsino like (bottom) NLPSs with different parameters. The parameter η is defined as $\mu = sgn(\mu)$.

Figure 1.5. In this model, gluino pairs are produced in the hard interaction, leading to decays to the NLSP under the emission of pairs of bottom quark pairs. The branching fractions for the $\tilde{\chi}_1^0$ to photons and Z bosons are again set to 50% each.

1.3.3 Status of SUSY searches at the Large Hadron Collider

Searches for SUSY have been performed since years at the LEP experiment [35], the Tevatron collider [36], and in the LHC RunI data [37]. Although some promising excesses have been observed for example in the opposite-sign dilepton channel [38], no clear evidences for SUSY or other BSM theories have been found. Currently SUSY is also constrained by precision measurements of the Higgs boson properties as mentioned above, and by the

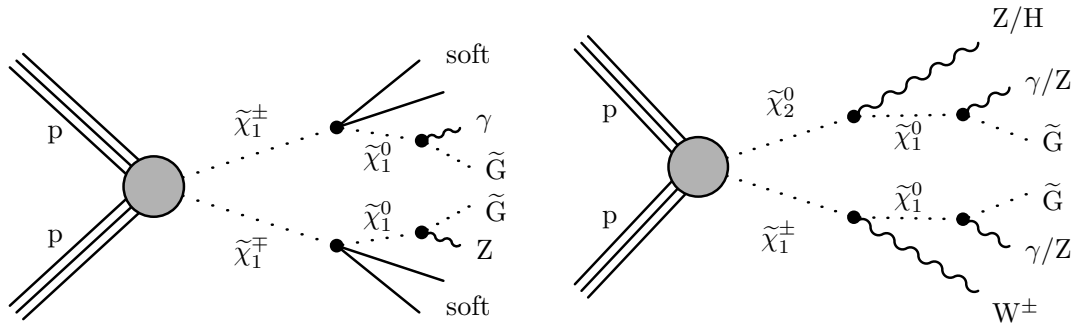

Figure 1.4: Diagram of the TChiZG scenario with chargino pair production, where the charginos decay to neutralinos under soft emission of offshell W bosons, (left). Also, the chargino-neutralino production is possible. The most dominant production process with a wino-like $\widetilde{\chi}_1^+$ and $\widetilde{\chi}_2^0$ and a bino-like $\widetilde{\chi}_1^0$ of the full GMSB model, (right).

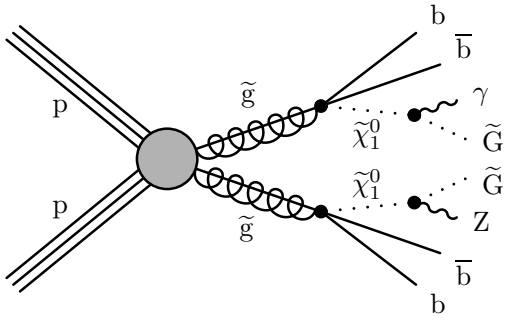

Figure 1.5: The Feynman diagram for the T5bbbbZG scenario with pair production of gluinos in the hard process, leading to decays to neutralinos under the emission of b quarks.

observation of the $B_S^0 \to \mu^-\mu^+$ decay by the CMS and LHCb collaborations [39]. Direct searches for SUSY in terms of SMS interpretations excluded gluino pair production up to gluino masses of 2 TeV [40], squark pair production up to squark masses of 1500 GeV and sbottom (stop) masses of 1500 GeV [41] (1200 GeV [42]) respectively. The production of electroweakinos is excluded for chargino/neutralino masses up to ≈ 1.1 TeV [43]. Regarding GMSB scenarios, the currently most stringent exclusion limits obtained by the CMS collaboration [44] are shown in Figure 1.6. The presented results are based on the

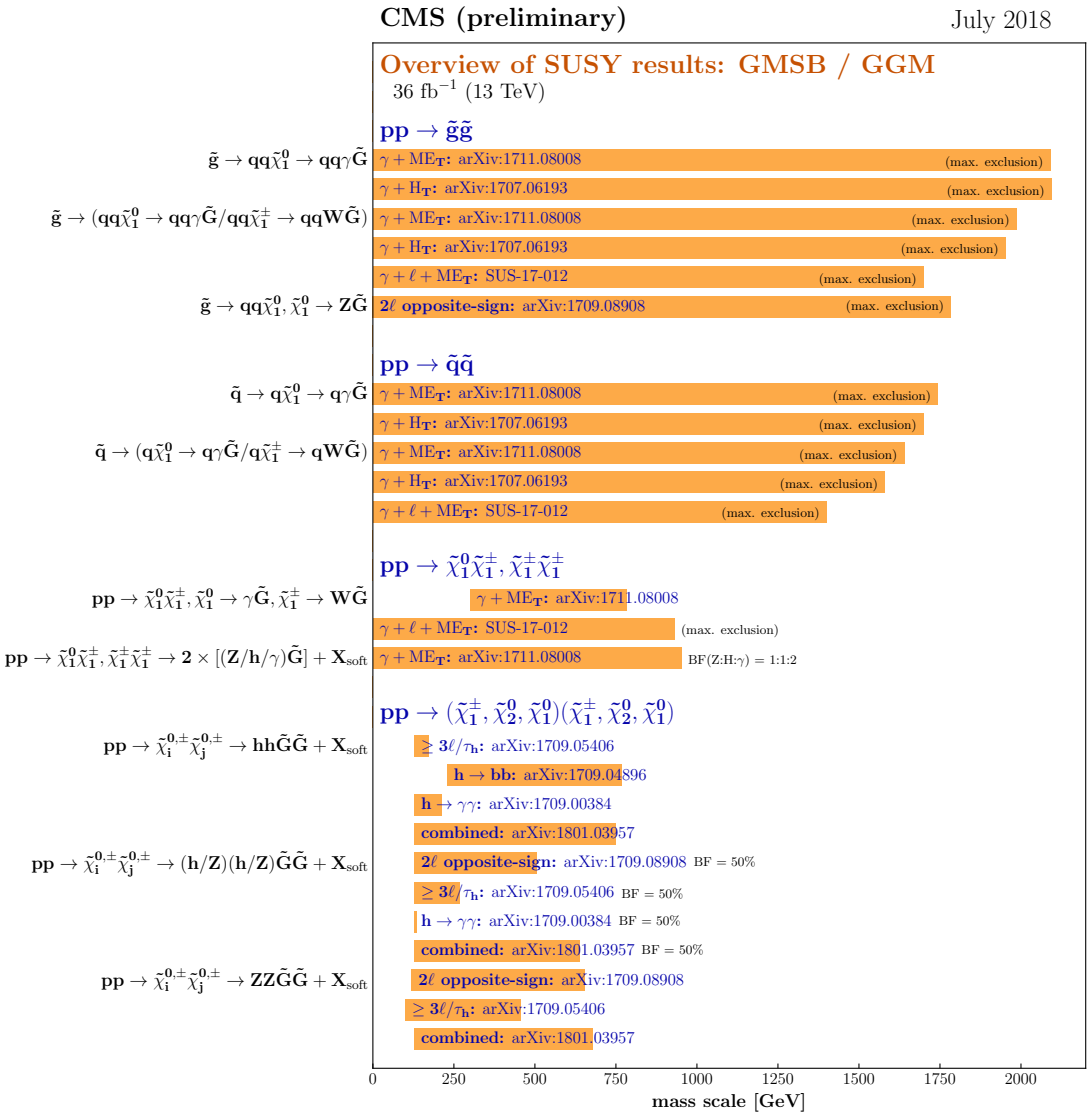

Selection of observed limits at 95% C.L. (theory uncertainties are not included). Probe **up to** the quoted mass limit for light LSPs unless stated otherwise. The quantities ΔM and x represent the absolute mass difference between the primary sparticle and the LSP, and the difference between the intermediate sparticle and the LSP relative to ΔM, respectively, unless indicated otherwise.

Figure 1.6: Mass exclusion limits for simplified models in the context of GMSB [45].

2016 proton-proton collision data recorded with the CMS detector in 2016, corresponding to an integrated luminosity of 36 fb^{-1} with an center-of-mass energy of $\sqrt{s} = 13$ TeV.

Searches similar to the one presented in this thesis, exclude electroweakino production scenarios up to $\approx 900\,\text{GeV}$, if final states tagged with a high energetic photon and large missing transverse momentum are analyzed [46]. Searches targeting the single lepton plus photon final state [47] have set lower limits. Strong exclusions for gluino and squark pair production scenarios are set by searches targeting events with large hadronic activity and photons [48], and photons in corresponding with high b-jet multiplicity [49] up to $\approx 2.2\,\text{TeV}$. gluino masses and 1.8 TeV squark masses.
Despite the high exclusion limits set by CMS and ATLAS analyzes [50–52] in comparable ways, large regions of phasespace remain unexplored. But since supersymmetry is not one specific model, and the phenomenology of SUSY is very rich, including scenarios with R-parity violation, compressed mass spectra, long-lived particles and displaced vertices, and all those described in different breaking scenarios, the search for SUSY stays interesting. Nevertheless, although the sparticle masses are not predicted by theory, natural SUSY scenarios without great finetuning should lead to sparticle masses in the order of $\mathcal{O}(\,\text{TeV})$, which are accessible at the LHC [53].

Chapter 2

The Experiment

In this chapter, the relevant experimental setup is explained. Starting with the description of the Large Hadron Collider (LHC), which is responsible for the acceleration of the proton beams, after that the Compact Muon Solenoid (CMS) experiment and detector with all important subdetector components is explained.

2.1 The large hadron collider

The Large Hadron Collider [54, 55], located at the European Organization of Nuclear Research (CERN) near Geneva in Switzerland, is the worlds largest hadron collider. The design center-of-mass energy for the proton-proton collisions is $\sqrt{s} = 14\,\text{TeV}$, while the LHC started operating in 2010 with an energy of 7 TeV. After running also in 2011 at 7 TeV, the energy was increased for the 2012 run period to 8 TeV. After that, the end of RunI, and after the first long shutdown, the LHC started running again in 2015 with an increased center-of-mass energy of 13 TeV. This setup was maintained trough the whole RunII until the end of 2018. In the following, the LHC will be upgraded again in the long shutdown II, so that with the beginning of 2021 it is planned to start operating with the design energy of 14 TeV. In addition the LHC is capable of accelerating lead ions with an energy of 2.76 TeV per nucleon.
The LHC is a synchroton collider built in a tunnel with a circumference of 27 km, which was already used for the Large Electron Positron collider (LEP) [56] in the past. The proton beams are accelerated using various preacceleators, such as the Booster, Proton Synchroton (PS), and the Super Proton Synchroton (SPS), delivering an proton energy of 450 GeV before entering the main storage ring. Four main experiments are located at the LHC, each built around one of the four collisions points. These namely are: CMS (Compact Muon Solenoid) [44], ATLAS (A Toroidal LHC Apparatus) [57], ALICE (A Large Ion Collider Experiment) [58], and LHCb (LHC Beauty) [59]. CMS and ATLAS were designed to be independent experiments looking both for BSM physics, measure precisely properties of the SM, and improve the knowledge on the Higgs sector. Besides those tasks, they also analyze lead ion collisions to gain a deeper understanding of the strong interaction. The tasks of ALICE include studies on the quark-gluon-plasma, where the confinement is abrogated, leading to asymptotically free quarks and gluons. LHCb investigates mainly mesons, that include charm and bottom quarks, to perform precision

measurements of the SM and indirectly look for $\mathcal{CP}$-violation and hints for new physics. The asymmetric detector design of LHCb favors such studies, since the forward region of particle flying close to the beam axis, is enriched with that kind of events. A schematic sketch of the LHC apparatus including the four big experiment locations and interaction points, and the preaccelerators, is shown in Figure 2.1.

As the protons are accelerated to an energy of 450 GeV, they are injected as bunches

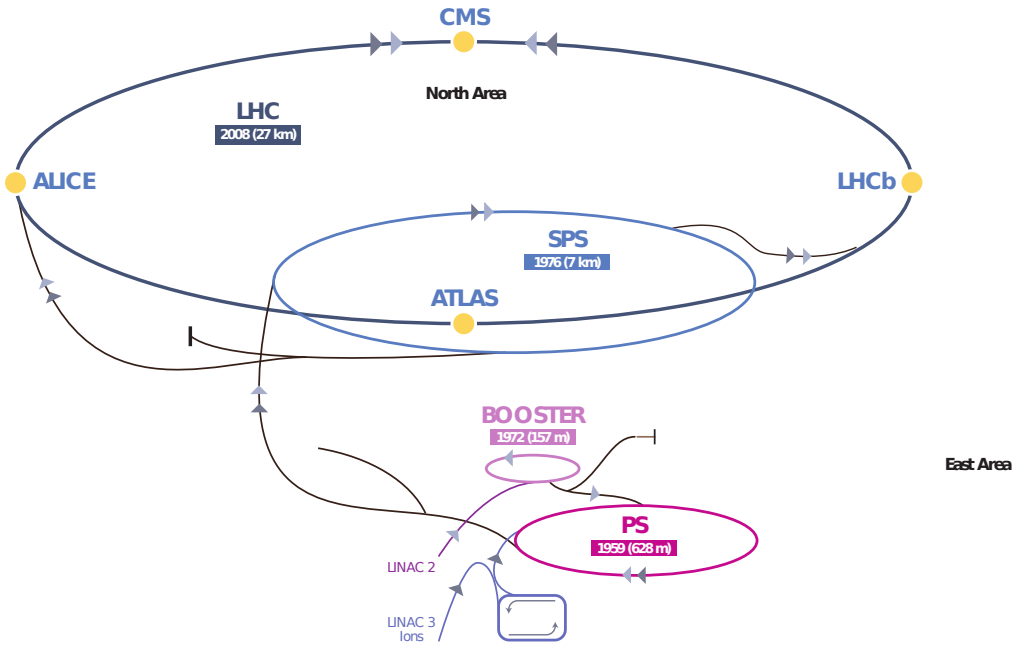

Figure 2.1: A sketch of the total LHC accelerator complex [60]. The four main experiments are marked as yellow dots, and the preacceleators are also shown.

of approximately $N = 1.1 \cdot 10^{10}$ particles into the two beam pipes counter rotating in intervals of 25 ns. To achieve a center-of-mass energy of 13 TeV, each beam has to reach an energy of 6.5 TeV. Therefore, superconducting cavities operating at 400 MHz accelerate the protons, and dipole magnets force the beams on their orbital path. Higher order multipoles are needed to focus the beam and correct for different beam and magnetic effects. One important quantity to characterize a collider is the instantaneous luminosity L, because the rate of a distinct scattering process is proportional to L. It can be defined as

$$L = \frac{N_b^2 n_b f_{rev} \gamma}{4\pi\epsilon\beta^*} F, \tag{2.1}$$

where N_b is the number of particles per bunch, n_b the number of bunches, f_{rev} the revolution frequency, γ the relativistic Lorentz factor, ϵ the normalized transverse emmitance of the beam, β^* the beta function at the interaction point, and F a geometrical factor accounting for the cross section angles of the beams. The instantaneous Luminosity $Lumi$ is related to L via

$$\mathcal{L} = \int L dt. \tag{2.2}$$

And the number of events N for a given process with cross section σ is given by

$$N = \mathcal{L} \cdot \sigma. \tag{2.3}$$

In 2016 the LHC provided a total integrated luminosity of $40.82\,\mathrm{pb}^{-1}$, while the CMS detector recorded $37.76\,\mathrm{pb}^{-1}$, and $35.92\,\mathrm{pb}^{-1}$ were validated to be used for physics analysis [61].

2.2 The compact muon solenoid detector

The data used in this thesis was recorded by the CMS detector [44, 62] in 2016. The CMS detector is a multi-purpose detector housing different subdetector components, namely being from inside to outside the tracker system including a pixel and the silicon strip detector, the electromagnetic calorimeter, the hadronic calorimeter, followed by the solenoid and the muon system. A cross section picture of the open CMS detector is shown in Figure 2.2. In the following each subdetector and the trigger system will be briefly explained. TODO September 26, 2018: RICHTIG machen oder anders BILD The coordinate system used to describe the detector is originated at the interaction point, and the z-axis points in the direction of the beam axis. The y-axis point upwards, while the x-axis points to center of the LHC ring. To exploit the underlying symmetry of the detector, a transformation to an angular coordinate system is chosen. The azimuthal angle ϕ is measured in the x-y plane, while $\phi = 0$ equals the direction of the x-axis, and ϕ ranges from $-\pi$ to π. The polar angle θ is measured from the positive z-axis, and the pseudorapidity η can be introduced

$$\eta = -\ln\left(\tan\left(\frac{\theta}{2}\right)\right). \tag{2.4}$$

The advantage in using η instead of θ is, that differences in θ are invariant under Lorentz-boosts along the beam axis.
Most of the subdetectors are divided in a low η part (barrel), and two high η parts (endcaps). Each of the subdetectors is designed to measure special properties of different particle types, to ensure both a good particle distinction and identification, and precise measurements of energy, momenta, and trajectories.

2.2.1 Tracker system

The most inner part of the CMS detector is the inner tracker and it consists of two main components, a silicon pixel and a silicon strip detector[1]. Both components enclose parts parallel to the beam pipe in the barrel, and parts orthogonal to the beam axis in the endcaps. They cover a length of 5.8 m and a diameter of 2.5 m. A sketch of the total inner track is shown in Figure 2.3. The tracker is designed to perform a precise measurement of particle trajectories and identification of primary and secondary vertices. Therefore, a high granularity and fast response is needed. The silicon pixel subcomponent is built of

[1] The silicon pixel detector was replaced at the end of the 2016 run. Since in this thesis only 2016 data is used, only the former detector is described.

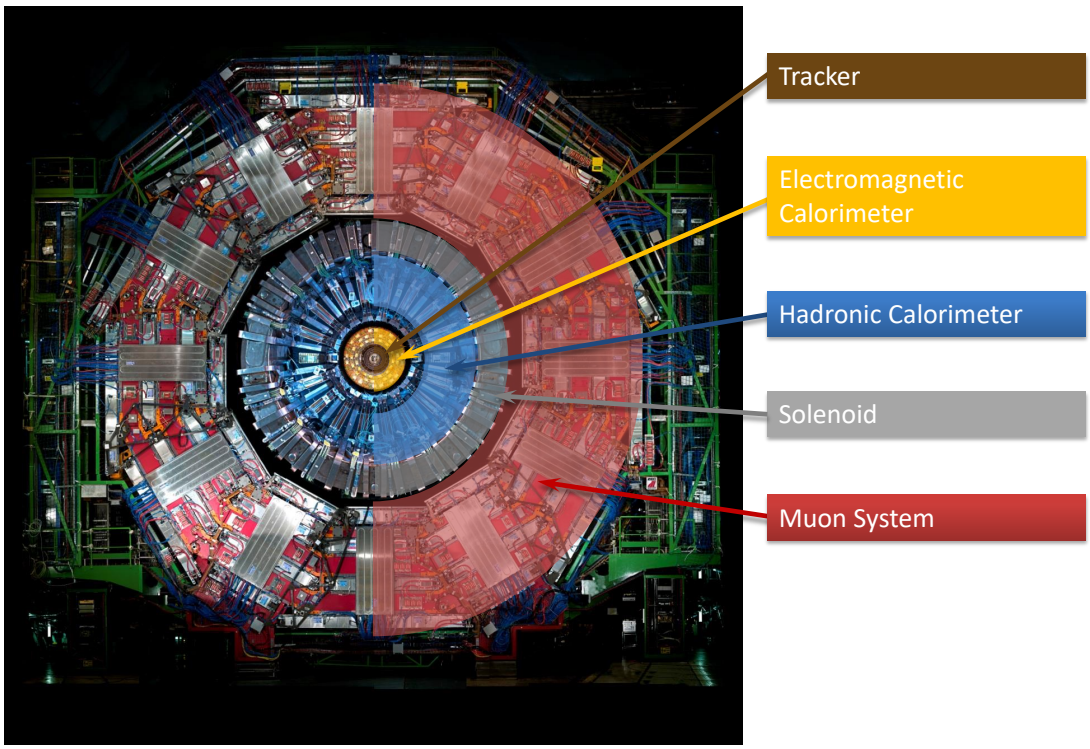

Figure 2.2: A cross section picture of the open CMS detector [63]. The important parts are labeled.

three barrel layers (the closest at a radial distance of 4.4 cm to the beam pipe) and two endcap disks, covering a total area size of around 1 m^2. Each of the ≈ 66 million silicon pixel cells has a size of $100x150\,\mu m^2$. This enables good resolution in all orientations independent of the track direction.
The silicon strip detector consists of four strip layers in the inner (TIB), and six layers in the outer part (TOB). In the direction of the endcaps, it is built of three inner disk layers (TID), and nine layer in the outer part (TEC).
The inner tracker in total covers a range of $|\eta| < 2.5$ and has a size of around 200 m^2. The performance of the tracker yields a momentum resolution for muons of a transverse momentum of ≈ 100 GeV of $1-2\%$ in $|\eta| < 1.6$. At higher pseudorapidities the momentum resolution decreases due to a lower granularity.

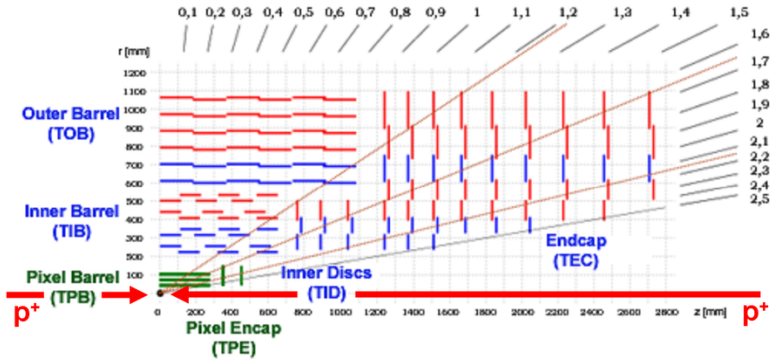

Figure 2.3: A sketch of one quadrant of the CMS inner tracker [64].

2.2.2 Electromagnetic calorimeter

Around the tracker, the second subdetector of CMS is the electromagnetic calorimeter (ECAL). Its main purpose is to measure the energy of electrons and photons, which behave very similar in the detector. Together with the measurements of the tracker, a differentiation between electrons and photons can be performed. It is made homogeneously of lead-tungstate ($PbWO_4$) crystals, that emit light proportional to the deposited energy of trespassing particles in an electromagnetic shower. The emitted light, which is located in the visible spectrum, is measured by avalanche photomultipliers. The material of lead-tungstate was chosen due to its high density, short Molière radius of 2.2 cm characterizing the shower width, and short radiation length of 0.89 cm. Another big advantage of $PbWO_4$ is she short scintillation time. In a time window of 25 ns most of the visible light (≈ 80%) is emitted, thus suiting very well the bunch spacing of 25 ns. The crystals have a length of 23 cm, matching 25.8 radiation lengths. So in total both a compact format and a high granularity could be maintained.
The ECAl is divided into a barrel (EB: $|\eta| < 1.479$) and an endcap part (EE: $1.479 < |\eta| < 3.0$), as can be seen in Figure 2.4. The total energy resolution of the ECAL is determined

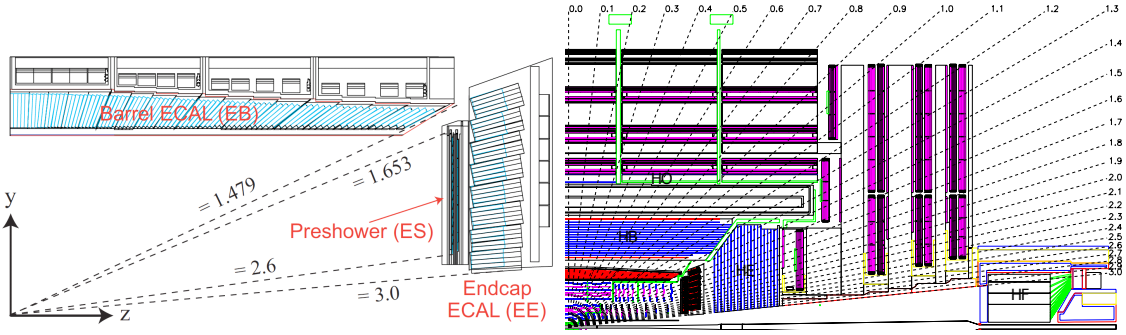

Figure 2.4: A sketch of one quadrant of the CMS detector for the ECAL (left) [65], and HCAL (right) [44].

to be

$$\left(\frac{\sigma_E}{E}\right)^2 = \left(\frac{2.8\%}{\sqrt{E[\,\mathrm{GeV}]}}\right)^2 + \left(\frac{0.12}{E[GeV]}\right)^2 + (0.30\%)^2, \tag{2.5}$$

where the first term covers stochastic effects due to the Poissionian distributed number of created scintillation photons, and the second term combines noise effects both from the electronics and the multiple collisions per bunch-crossing (pile-up). The third term covers constant effects, such as intercalibration effects between the crystals and energy leakage [66].
An additional preshower detector is installed in front of the ECAL endcap, to identify photons coming from meson decays.

2.2.3 Hadronic calorimeter

The hadronic calorimeter (HCAL), which is designed for the energy measurement of hadrons, consists also of a barrel (HB) and endcap parts (HE). It is placed between the ECAL at a radius of 1.77 m, and the coil at a radius of 2.95 m. An additional outer barrel part with lower granularity (HO) extends the HCAL outside of the solenoid making use of its stopping power, while the hadron forward (HF) is installed to cover high pseudorapidity ranges. The barrel part covers pseudorapidities in the range of $|\eta| < 1.4$, while the HCAL endcap together with the outer HCAL covers the range of $1.3 < |\eta| < 3$.
In contrast to the homogeneous ECAL, the HCAL barrel consists of alternating layers of brass and plastic scintillating material. The front and backplates are made of steel. Hence, the brass plates stop the incoming particles, and the energy deposit is measured in the form of hadronic showers creating scintillation light in the plastic layers. The outer HCAL makes use of the same principle, but uses in addition the stopping power of the solenoid. The hadron forward, covering pseudorapidity ranges of $3|\eta| < 5.2$, needs to be more radiation hard in comparison to the rest of the HCAL, since the energy deposit in the forward region is much higher, is therefore a Cherenkov detector made of quartz fibres. A total sketch of the HCAL can be seen in Figure 2.4.

2.2.4 The solenoid

To measure the momentum of the charged particles properly, it is crucial to have bended trajectories. The resolution of the momentum measurement at very high energies is directly proportional measurement of the curvature of the trajectory, a strong magnetic field is needed. Hence, this is provided by a superconducting NbTi magnet, cooled down to 4.8 K, inducing a magnetic field of 3.8 T.

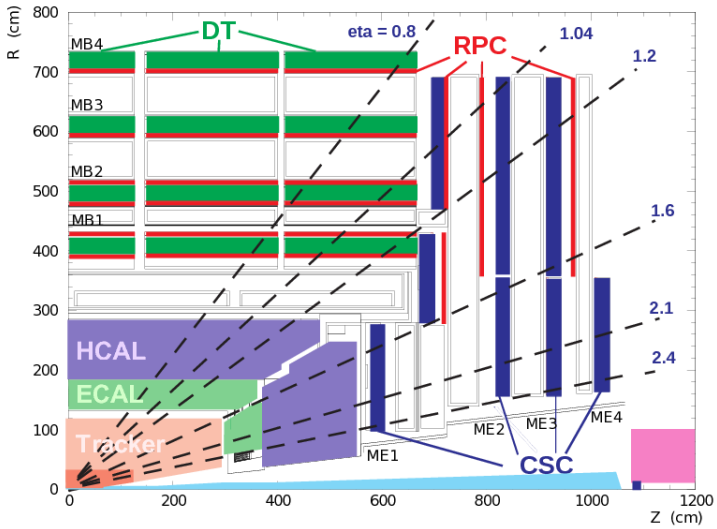

Figure 2.5: A sketch of one quadrant of the CMS detector is shown with the main detector components [67].

2.2.5 Muon system

The most outside part of the CMS detector is the muon system. Because all other particles besides muons should be stopped in the inner layers, muons are the only particles trespassing and leaving the muon system. Three different types of detectors are used to measure and identify muons. The barrel part ($|\eta| < 1.2$) is covered by four stations of drift tubes (DT). Cathode strip chambers (CSC) are covering the endcap at pseudorapidity $0.9 < |\eta| < 2.4$, because in this region a higher muon rate is expected, and CSCs in contrast to DTs have a faster response time and are more radiation hard. In ost of the parts the muon efficiency is above 95%, with the misidentification is below 1%. The muon momentum resolution, dependent on the η region, varies between 1% to 6% for muons with a transverse momentum below 100 GeV, and is in the order of 10% for TeV muons [68]. A third type of detector components, namely six layers of resistive plate chambers (RPC), are installed in the pseudorapidity range of $< \eta| < 1.6$. Because they show both good time resolution and fast response time, they are mainly used for triggering purposes. The structure of the muon system can be seen in Figure 2.5.

2.2.6 Trigger system

Because collisions take place every 25 ns, and therefore at a rate of 40 MHz, it is not achievable to read out and store all event details. To keep only physically interesting events and reduce the rate of events to be saved, a trigger system consisting of two stages is implemented [69]. It is composed of the hardware based level 1 triggers (L1), and the software based high level triggers (HLT). Since the L1 trigger needs to deliver decisions in a very short time window, it uses only information provided by the calorimeters and the muon chambers. Usually first requirements on the event, such as a minimal deposited transverse energy, and first estimates for electron and muon candidates are imposed. The L1 trigger reduces the event to a rate of ≈ 100 kHz.
A more complex decision taking is performed by the HLT trigger. It has full access to the total readout of all subdetectors, and therefore performs selections close to the offline analysis. It reduces the event rate to $\mathcal{O}(400H^0)$.
Using the decisions of the HLT, events are categorized into different subsets, based on event kinematics and the trigger objects.

Bibliography

[1] F. Pisano and N. O. Reis, "Natural units, numbers and numerical clusters", arXiv:hep-ph/0112097.

[2] A. Pich, "The Standard model of electroweak interactions", in *The Standard model of electroweak interactions*, pp. 1–49. 2008. arXiv:0705.4264. [,1(2007)].

[3] A. Einstein, "The Foundation of the General Theory of Relativity", *Annalen Phys.* **49** (1916), no. 7, 769–822, doi:10.1002/andp.200590044,10.1002/andp.19163540702. [,65(1916)].

[4] Particle Data Group Collaboration, "Review of Particle Physics", *Chin. Phys.* **C40** (2016), no. 10, 100001, doi:10.1088/1674-1137/40/10/100001.

[5] K. G. Wilson, "Confinement of quarks", *Phys. Rev. D* **10** (Oct, 1974) 2445–2459, doi:10.1103/PhysRevD.10.2445.

[6] S. Weinberg, "Effects of a Neutral Intermediate Boson in Semileptonic Processes", *Phys. Rev. D* **5** (Mar, 1972) 1412–1417, doi:10.1103/PhysRevD.5.1412.

[7] S. Weinberg, "A Model of Leptons", *Phys. Rev. Lett.* **19** (Nov, 1967) 1264–1266, doi:10.1103/PhysRevLett.19.1264.

[8] A. Salam and J. Ward, "Electromagnetic and weak interactions", *Physics Letters* **13** (1964), no. 2, 168 – 171, doi:https://doi.org/10.1016/0031-9163(64)90711-5.

[9] S. L. Glashow, "Partial-symmetries of weak interactions", *Nuclear Physics* **22** (1961), no. 4, 579 – 588, doi:https://doi.org/10.1016/0029-5582(61)90469-2.

[10] P. W. Higgs, "Broken Symmetries and the Masses of Gauge Bosons", *Phys. Rev. Lett.* **13** (Oct, 1964) 508–509, doi:10.1103/PhysRevLett.13.508.

[11] F. Englert and R. Brout, "Broken Symmetry and the Mass of Gauge Vector Mesons", *Phys. Rev. Lett.* **13** (Aug, 1964) 321–323, doi:10.1103/PhysRevLett.13.321.

[12] G. S. Guralnik, C. R. Hagen, and T. W. B. Kibble, "Global Conservation Laws and Massless Particles", *Phys. Rev. Lett.* **13** (Nov, 1964) 585–587, doi:10.1103/PhysRevLett.13.585.

[13] CMS Collaboration, "Observation of a new boson at a mass of 125 GeV with the

CMS experiment at the LHC", *Phys. Lett.* **B716** (2012) 30–61, doi:10.1016/j.physletb.2012.08.021, arXiv:1207.7235.

[14] ATLAS Collaboration, "Observation of a new particle in the search for the Standard Model Higgs boson with the ATLAS detector at the LHC", *Phys. Lett.* **B716** (2012) 1–29, doi:10.1016/j.physletb.2012.08.020, arXiv:1207.7214.

[15] CMS Collaboration, "Precise determination of the mass of the Higgs boson and tests of compatibility of its couplings with the standard model predictions using proton collisions at 7 and 8 TeV", *Eur. Phys. J.* **C75** (2015), no. 5, 212, doi:10.1140/epjc/s10052-015-3351-7, arXiv:1412.8662.

[16] CMS Collaboration Collaboration, "Observation of $t\bar{t}H$ Production", *Phys. Rev. Lett.* **120** (Jun, 2018) 231801, doi:10.1103/PhysRevLett.120.231801.

[17] CMS Collaboration, "Observation of the Higgs boson decay to a pair of τ leptons with the CMS detector", *Phys. Lett.* **B779** (2018) 283–316, doi:10.1016/j.physletb.2018.02.004, arXiv:1708.00373.

[18] CMS Collaboration, "Observation of Higgs boson decay to bottom quarks", *Submitted to: Phys. Rev. Lett.* (2018) arXiv:1808.08242.

[19] Planck Collaboration, "Planck 2015 results. XIII. Cosmological parameters", *Astron. Astrophys.* **594** (2016) A13, doi:10.1051/0004-6361/201525830, arXiv:1502.01589.

[20] R. Massey, T. Kitching, and J. Richard, "The dark matter of gravitational lensing", *Rept. Prog. Phys.* **73** (2010) 086901, doi:10.1088/0034-4885/73/8/086901, arXiv:1001.1739.

[21] M. Persic, P. Salucci, and F. Stel, "The Universal rotation curve of spiral galaxies: 1. The Dark matter connection", *Mon. Not. Roy. Astron. Soc.* **281** (1996) 27, doi:10.1093/mnras/281.1.27,10.1093/mnras/278.1.27, arXiv:astro-ph/9506004.

[22] L. Canetti, M. Drewes, and M. Shaposhnikov, "Matter and Antimatter in the Universe", *New J. Phys.* **14** (2012) 095012, doi:10.1088/1367-2630/14/9/095012, arXiv:1204.4186.

[23] G. R. Farrar and M. E. Shaposhnikov, "Baryon asymmetry of the universe in the minimal Standard Model", *Phys. Rev. Lett.* **70** (1993) 2833–2836, doi:10.1103/PhysRevLett.71.210.2,10.1103/PhysRevLett.70.2833, arXiv:hep-ph/9305274. [Erratum: Phys. Rev. Lett.71,210(1993)].

[24] A. D. Sakharov, "Violation of CP Invariance, C asymmetry, and baryon asymmetry of the universe", *Pisma Zh. Eksp. Teor. Fiz.* **5** (1967) 32–35, doi:10.1070/PU1991v034n05ABEH002497. [Usp. Fiz. Nauk161,no.5,61(1991)].

[25] M. C. Gonzalez-Garcia and Y. Nir, "Neutrino masses and mixing: Evidence and implications", *Rev. Mod. Phys.* **75** (2003) 345–402,

doi:10.1103/RevModPhys.75.345, arXiv:hep-ph/0202058.

[26] J. Wess and B. Zumino, "Supergauge Transformations in Four-Dimensions", *Nucl. Phys.* **B70** (1974) 39–50, doi:10.1016/0550-3213(74)90355-1. [,24(1974)].

[27] S. P. Martin, "A Supersymmetry primer", doi:10.1142/9789812839657_0001,10.1142/9789814307505_0001, arXiv:hep-ph/9709356. [Adv. Ser. Direct. High Energy Phys.18,1(1998)].

[28] SNO Collaboration, "Constraints on nucleon decay via 'invisible' modes from the Sudbury Neutrino Observatory", *Phys. Rev. Lett.* **92** (2004) 102004, doi:10.1103/PhysRevLett.92.102004, arXiv:hep-ex/0310030.

[29] P. Meade, N. Seiberg, and D. Shih, "General Gauge Mediation", *Prog. Theor. Phys. Suppl.* **177** (2009) 143–158, doi:10.1143/PTPS.177.143, arXiv:0801.3278.

[30] P. Meade, M. Reece, and D. Shih, "Prompt Decays of General Neutralino NLSPs at the Tevatron", *JHEP* **05** (2010) 105, doi:10.1007/JHEP05(2010)105, arXiv:0911.4130.

[31] S. Dimopoulos, S. D. Thomas, and J. D. Wells, "Sparticle spectroscopy and electroweak symmetry breaking with gauge mediated supersymmetry breaking", *Nucl. Phys.* **B488** (1997) 39–91, doi:10.1016/S0550-3213(97)00030-8, arXiv:hep-ph/9609434.

[32] S. Ambrosanio et al., "Search for supersymmetry with a light gravitino at the Fermilab Tevatron and CERN LEP colliders", *Phys. Rev.* **D54** (1996) 5395–5411, doi:10.1103/PhysRevD.54.5395, arXiv:hep-ph/9605398.

[33] D. Alveset al., "Simplified models for LHC new physics searches", *Journal of Physics G: Nuclear and Particle Physics* **39** (2012), no. 10, 105005.

[34] CMS Collaboration Collaboration, "Interpretation of searches for supersymmetry with simplified models", *Phys. Rev. D* **88** (Sep, 2013) 052017, doi:10.1103/PhysRevD.88.052017.

[35] S. Ask, "A Review of the supersymmetry searches at LEP", in *38th Rencontres de Moriond on Electroweak Interactions and Unified Theories Les Arcs, France, March 15-22, 2003*. 2003. arXiv:hep-ex/0305007.

[36] X. P. Bueso, "Supersymmetry Searches at the Tevatron and the LHC Collider Experiments", in *Proceedings, 31st International Conference on Physics in collisions (PIC 2011): Vancouver, Canada, August 28-September 1, 2011*. 2011. arXiv:1112.1723.

[37] C. Autermann, "Experimental status of supersymmetry after the LHC Run-I", *Prog. Part. Nucl. Phys.* **90** (2016) 125–155, doi:10.1016/j.ppnp.2016.06.001, arXiv:1609.01686.

[38] CMS Collaboration, "Search for Physics Beyond the Standard Model in Events with

Two Leptons, Jets, and Missing Transverse Momentum in pp Collisions at sqrt(s) = 8 TeV", *JHEP* **04** (2015) 124, doi:10.1007/JHEP04(2015)124, arXiv:1502.06031.

[39] LHCb, CMS Collaboration, "Observation of the rare $B_s^0 \to \mu^+\mu^-$ decay from the combined analysis of CMS and LHCb data", *Nature* **522** (2015) 68–72, doi:10.1038/nature14474, arXiv:1411.4413.

[40] CMS Collaboration, "Search for Physics Beyond the Standard Model in Events with High-Momentum Higgs Bosons and Missing Transverse Momentum in Proton-Proton Collisions at 13 TeV", *Phys. Rev. Lett.* **120** (2018), no. 24, 241801, doi:10.1103/PhysRevLett.120.241801, arXiv:1712.08501.

[41] CMS Collaboration, "Search for new phenomena in final states with two opposite-charge, same-flavor leptons, jets, and missing transverse momentum in pp collisions at $\sqrt{s} = 13$ TeV", *JHEP* **03** (2018) 076, doi:10.1007/s13130-018-7845-2,10.1007/JHEP03(2018)076, arXiv:1709.08908.

[42] CMS Collaboration, "Search for top squarks and dark matter particles in opposite-charge dilepton final states at $\sqrt{s} = 13$ TeV", *Phys. Rev.* **D97** (2018), no. 3, 032009, doi:10.1103/PhysRevD.97.032009, arXiv:1711.00752.

[43] CMS Collaboration, "Search for electroweak production of charginos and neutralinos in multilepton final states in proton-proton collisions at $\sqrt{s} = 13$ TeV", *JHEP* **03** (2018) 166, doi:10.1007/JHEP03(2018)166, arXiv:1709.05406.

[44] T. C. Collaborationet al., "The CMS experiment at the CERN LHC", *Journal of Instrumentation* **3** (2008), no. 08, S08004.

[45] C. Collaboration, "CMS Supersymmetry Physics Results".

[46] CMS Collaboration, "Search for gauge-mediated supersymmetry in events with at least one photon and missing transverse momentum in pp collisions at $\sqrt{s} = 13$ TeV", *Phys. Lett.* **B780** (2018) 118–143, doi:10.1016/j.physletb.2018.02.045, arXiv:1711.08008.

[47] CMS Collaboration Collaboration, "Search for supersymmetry using events with a photon, a lepton, and missing transverse momentum in pp collisions at sqrt(s) = 13 TeV", Technical Report CMS-PAS-SUS-17-012, CERN, Geneva, 2018.

[48] CMS Collaboration, "Search for supersymmetry in events with at least one photon, missing transverse momentum, and large transverse event activity in proton-proton collisions at $\sqrt{s} = 13$ TeV", *JHEP* **12** (2017) 142, doi:10.1007/JHEP12(2017)142, arXiv:1707.06193.

[49] CMS Collaboration Collaboration, "Search for supersymmetry in events with a photon, jets, and missing transverse momentum in proton-proton collisions at 13 TeV", Technical Report CMS-PAS-SUS-18-002, CERN, Geneva, 2018.

[50] ATLAS Collaboration, "Search for supersymmetry in events with four or more leptons in $\sqrt{s} = 13$ TeV pp collisions with ATLAS", *Phys. Rev.* **D98** (2018), no. 3, 032009, doi:10.1103/PhysRevD.98.032009, arXiv:1804.03602.

[51] ATLAS Collaboration, "Search for pair production of higgsinos in final states with at least three b-tagged jets in $\sqrt{s} = 13$ TeV pp collisions using the ATLAS detector", *Submitted to: Phys. Rev.* (2018) arXiv:1806.04030.

[52] ATLAS Collaboration, "Search for photonic signatures of gauge-mediated supersymmetry in 13 TeV pp collisions with the ATLAS detector", *Phys. Rev. D* **97** (2018), no. 9, 092006, doi:10.1103/PhysRevD.97.092006, arXiv:1802.03158.

[53] J. L. Feng, "Naturalness and the Status of Supersymmetry", *Ann. Rev. Nucl. Part. Sci.* **63** (2013) 351–382, doi:10.1146/annurev-nucl-102010-130447, arXiv:1302.6587.

[54] L. R. F. Castillo, "The Large Hadron Collider", in *The Search and Discovery of the Higgs Boson*, 2053-2571, pp. 3–1 to 3–9. Morgan Claypool Publishers, 2015.

[55] L. Evans and P. Bryant, "LHC Machine", *Journal of Instrumentation* **3** (2008), no. 08, S08001.

[56] G. Bachy et al., "The LEP collider", *Part. Accel.* **26** (1990) 19–32.

[57] T. A. Collaborationet al., "The ATLAS Experiment at the CERN Large Hadron Collider", *Journal of Instrumentation* **3** (2008), no. 08, S08003.

[58] T. A. Collaborationet al., "The ALICE experiment at the CERN LHC", *Journal of Instrumentation* **3** (2008), no. 08, S08002.

[59] T. L. Collaboration, A. A. A. Jr, L. M. A. Filho, and T. Ypsilantis, "The LHCb Detector at the LHC", *Journal of Instrumentation* **3** (2008), no. 08, S08005.

[60] E. Mobs, "The CERN accelerator complex - August 2018. Complexe des accÃ©lÃ©rateurs du CERN - AoÃ»t 2018",. General Photo, Modified.

[61] C. Collaboration, "Public CMS data quality information".

[62] CMS Collaboration CollaborationG. L. Bayatian, et al., "CMS Physics: Technical Design Report Volume 1: Detector Performance and Software". Technical Design Report CMS. CERN, Geneva, 2006. There is an error on cover due to a technical problem for some items.

[63] M. Hoch and M. Brice, "CMS experiment", (Aug, 2008). CMS Collection.

[64] V. Halyo, P. LeGresley, and P. Lujan, "Massively Parallel Computing and the Search for Jets and Black Holes at the LHC", *Nucl. Instrum. Methods Phys. Res., A* **744** (Sep, 2013) 54–60. 7 p. Comments: 11 pages, 9 figures.

[65] CMS Collaboration Collaboration, "The CMS ECAL performance with examples", Technical Report CMS-CR-2013-430, CERN, Geneva, Nov, 2013.

[66] C. Collaboration, "Performance and operation of the CMS electromagnetic calorimeter", *Journal of Instrumentation* **5** (2010), no. 03, T03010.

[67] CMS Collaboration, "CMS reconstruction improvement for the muon tracking by the RPC chambers", *PoS* **RPC2012** (2012) 045, doi:10.1088/1748-0221/8/03/T03001,10.22323/1.159.0045, arXiv:1209.2646. [JINST8,T03001(2013)].

[68] CMS Collaboration, "Performance of CMS muon reconstruction in pp collision events at $\sqrt{s} = 7$ TeV", *JINST* **7** (2012) P10002, doi:10.1088/1748-0221/7/10/P10002, arXiv:1206.4071.

[69] V. Khachatryanet al., "The CMS trigger system", *Journal of Instrumentation* **12** (2017), no. 01, P01020.